Asian Journal of Chemistry; Vol. 37, No. 11 (2025), 2668-2678
ASIAN JOURNAL OF CHEMISTRY
https://doi.org/10.14233/ajchem.2025.34621

Experimental and Theoretical Studies on (*E*)-4-Hydroxy-3-methoxy-5-((3-nitrophenyl)diazenyl)benzaldehyde: A Dichromic Azo Dye with pH-Responsive Applications

EKTA KUNDRA ARORA*, VIBHA SHARMA*, TIMOTHY GLADSTON, ANNRIYA TOM, ALEENA KUNJUMON, JESLIN MARY THOMAS, AYUSH GEORGE, ANITA SEBASTIAN, EVELYN MARIE and SHREYA RAWAT

Department of Chemistry, St. Stephen's College, University of Delhi, Delhi-110007, India

*Corresponding authors: E-mail: ekta.kundra@ststephens.edu; vibha.sharma@ststephens.edu

Received: 3 August 2025 *Accepted*: 7 September 2025 *Published online*: 27 October 2025 AJC-22153

An azo dye (*E*)-4-hydroxy-3-methoxy-5-((3-nitrophenyl)diazenyl)benzaldehyde (AD) was synthesized and characterized using elemental analysis (CHN), ^{1}H NMR, ^{13}C NMR, ATR-IR and mass spectrometry. The DFT calculations with B3LYP/6-311++g(d,p) (gas phase/ethanol) were performed with Gaussian 16 to understand the structural features, azo-hydrazone tautomerism and electronic absorption characteristics of the titled compound. Conformations were analyzed in the gas phase and in ethanol by a relaxed potential energy scan. The azo tautomer in ethanol was found to have the lowest energy (-1080.65601 Hartree). A comparison between the computed UV-Vis spectra using TD-DFT and the experimental spectra indicates that the azo and hydrazone tautomers coexist in equilibrium in ethanol. This alignment suggests the presence of both forms in solution, contributing to the observed spectral characteristics. The dye is pH-responsive and dichromic. It changes colour from pale yellow in acidic medium to orange in basic medium. The computed absorption spectrum of the azo (low pH form) and the enolate ion (high pH form) correlated well with the experimental results. Analysis of the molecular orbitals involved in the electronic transitions of the dye reveals that the new absorption peak observed in the enolate ion form (λ_{max} = 466 nm) arises from a combination of transitions, specifically from the HOMO to LUMO+1 and HOMO–1 to LUMO+1. This mixed character of transitions contribute to the distinct spectral feature associated with the enolate form. The dye was successfully tested as an effective indicator for strong acid-strong base titrations. It may further be developed as an optical switch for pH-responsive applications. The HOMO-LUMO gaps for the azo, hydrazone and enolate ion forms are 3.37, 2.82 and 2.33 eV, respectively.

Keywords: Acid-base titrations, Acidochromism, Azo dye, DFT, Dichromism, Tautomerism.

INTRODUCTION

The aromatic azo (-N=N-) compounds are versatile, strikingly coloured artificial organic dyes that have been used for centuries. Applications based on colour include use as food colorants, dyes for fabrics and leather, indicators in titrimetric analysis, chemosensors in analytical chemistry and cosmetics [1-3]. Photochromism, light-induced conversion from *trans*-(E) to *cis*-(Z) form, has wide applications in material sciences, biology, memory-based applications, bioimaging and capture and release of drugs [4-9]. Azobenzenes also exhibit notable nonlinear optical properties (NLO) [10-12]. The chromogenic properties of azo dyes enable spectrophotometric detection of metal ions and anions in solution [13-16]. Beyond colour-based applications, azo compounds are known to have antiviral, antifungal, antioxidant, antibacterial and DNA-binding abilities [2,17-21].

Azo dye synthesis is simple and is typically performed in an aqueous medium. Experiments as well as computational studies have been used to understand the substituent effects, tautomerism and solvatochromism in azo dyes and how they influence colour [22-26]. Azo dyes are recognized as smart and intelligent materials [27-31]. Recent innovations include the synthesis of a polyazo dye (a universal acid-base indicator) by diazotizing aniline and coupling it with sulfanilic acid and *N*,*N*-dimethylaniline [32]. Benzothiazole-based azo dyes have also emerged as low-pH optical sensors [33]. Notably, Bartwal *et al.* [34] have developed a pH-responsive ampyrone based azo dye that functions as a chemo-reversible colorimetric fluorescent probe for Al(III) ions in semi-aqueous medium [34]. Recently, Mestry *et al.* [28] synthesized vanillin-based imine-azo dyes that exhibited strong pH sensitivity and colour transitions, making them useful for smart packaging applications. Purwono *et al*. [35] have synthesized azo-imine derivatives of vanillin-based dye, which change colour above pH 9.

Classical methods like titrimetric analysis work well at higher concentrations and need no special calibration, making it a method of choice for cost-effective analysis of analytes [36,37]. Acid-base titrations rely extensively on visual indicators to determine the endpoint of a titration. The colour change is attributed to structural changes, *i.e.* electronic distribution within the weakly acidic or basic organic compound [36,38]. The ionized and non-ionized forms of the organic dyes have different colours. If the pH of the solution is less than pK_I, the acidic form dominates; if the pH is more than pK_I, the basic form dominates.

$$HI + H_2O \rightarrow I^- + H_3O^+ \quad (1)$$

$$pk_I = \frac{a_{I^-} \times a_{H_3O^+}}{a_{HI}} \quad (2)$$

Dichromic indicators exhibit a colour change interval (eqn. 3) influenced by factors such as human colour perception, the ionic strength of the medium and salt error. These variables can alter the apparent transition range and accuracy of the indicator in analytical applications.

$$\Delta pH = pK_I \pm 1 \quad (3)$$

This study investigates the use of (*E*)-4-hydroxy-3-methoxy-5-((3-nitrophenyl)diazenyl)benzaldehyde (AD) as a pH responsive indicator and computationally explores the structure property relationships of AD [39,40], an azo dye with a colour change near pH 7. Azo dyes such as methyl orange (pH 3.1-4.4) and methyl red (pH 4.4-6.2), which change colour well below pH 7, are suitable for strong acid-weak base titrations [38]. Most azo dye indicators shift colour in highly acidic or basic pH ranges. Phenolphthalein, a triphenylmethane dye, has a transition range of 8.2-10.0. AD differs from methyl orange and methyl red, mainly due to the nature and position of its substituents, which function as auxochromes. Unlike methyl orange and methyl red, AD exhibits inverse colorimetric behaviour, appearing yellow in acidic conditions and bright orange in basic conditions, with a distinct change near pH 7 (pK_a = 6.72 ± 0.02). We evaluate the potential of the titled compound AD as an indicator for a strong acid-strong base titration using varying concentrations of NaOH, HCl and $C_2O_4H_2$ and to our knowledge, this has not been previously reported. Computational analysis of AD offers insights into its electronic, optical and structural properties. We examine the structures of the azo, hydrazone and enolate forms to study their pH-dependent behaviour, calculate HOMO-LUMO gaps and compare the computational results with the experimental data. These results will help in designing new compounds based on this scaffold and improving their properties for targeted applications.

EXPERIMENTAL

All reagents were procured commercially and used as such. Sodium nitrite, 3-nitroaniline, N,N-dimethyl formamide, acetic acid, sodium bicarbonate and sodium hydroxide were purchased from Loba Chemie Pvt. Ltd., India. Vanillin was purchased from Central Drug House Pvt. Ltd., India, hydrochloric acid from Thermo-Fisher Scientific Pvt. Ltd. and potassium chloride from Avarice Industries, India.

Characterization: The IR spectrum was recorded on Nicolet iS50 FTIR Tri-detector, Gold flex spectrometer-Gold optics with 0.09 cm^{-1} resolution, DLaTGS detector with KBr window, Ge-on-KBr beam splitter (7800-350 cm^{-1}) 50 Build-in Diamond ATR module and scanning range 4000-400 cm^{-1}. The ^1H & ^{13}C NMR spectra in DMSO-d_6 were recorded on a JEOL, Model: JNM-ECZ 400S, 400 MHz instrument with TMS as the internal standard at 25 ºC. The mass spectrum was recorded on a Vanquish Neo UHPLC and Orbitrap Exploris 480 MS (Thermo-Scientific). Elemental analysis (CHN) was performed on Elementar Analysensysteme Germany, Model: Vario Micro Cube. The absorption spectra were measured using Labtronics UV-vis spectrophotometer, model no. LT-1900 double beam spectrophotometer, using a quartz cuvette with a path length of 1 cm.

Preparation of solutions: Buffer solutions (pH 1-13) were prepared by standard methods [37]. The dye was dissolved in ethanol (3×10^{-4} mol/L). Two drops of the dye solution were added to 2.5 mL of buffer solution (pH 1-13) taken in test tubes. The electronic absorption spectra of the solutions were recorded at room temperature.

Titration: Acid-base titrations were performed using different concentrations of HCl/$H_2C_2O_4$ as titrand and NaOH as titrant to assess the suitability of AD as an indicator. 10 mL of acid was pipetted in an Erlenmeyer flask and titrated against NaOH using two drops of AD as indicator. The comparative titrations were performed using two drops of phenolphthalein per titration as a standard indicator. Trials were repeated thrice and the mean and standard deviation for each type of acid-base titration was calculated.

Synthesis of (*E*)-4-hydroxy-3-methoxy-5-((3-nitrophenyl)benzaldehyde (AD): A mixture of 1.5 mL of distilled water and 1.5 mL of conc. HCl was prepared in a test tube and subsequently placed in an ice bath to maintain a low temperature during the reaction process. 3-Nitroaniline (0.6907 g, 5 mmol), $NaNO_2$ (0.3454 g, 5.1 mmol) and 1.5 mL of distilled water were added to a beaker and magnetically stirred while maintaining the temperature between 0-5 ºC, by placing the beaker in an ice bath. The contents of the test tube and beaker were mixed and stirred gently for 10 min. Vanillin (0.7607 g, 5.5 mmol) was added to 4 mL of 10% NaOH solution in a beaker and stirred magnetically. The beaker was then placed in an ice bath to maintain the temperature between 0-5 ºC. The contents of the two beakers were mixed and magnetically stirred for 10 min. Distilled water was added to the mixture and a suspension was obtained. The residue was Büchner-filtered, washed with distilled water, collected and left to air dry (**Scheme-I**). The crude product was subsequently recrystallized with ethanol. AD is maroon-red in colour, with a melting point range of 176-180 ºC. The yield of AD is 80%. Elemental analysis found (calculated): C: 55.59 (55.82); H: 3.477 (3.68); N: 14.28 (13.95) %.

Computational studies: All theoretical studies were performed using the Gaussian program package Gaussian 16, revision C.01 with GaussView 6 [41,42]. A relaxed potential energy surface scan was used to study conformations in the gas phase and ethanol. Geometry optimizations and frequency calculations of the azo, hydrazone and deprotonated form of AD in the gas phase and ethanol were performed by DFT using the RB3LYP functional, 6-311++g(d,p) basis sets for all atoms and the polar continuum model (PCM) to mimic the solvent

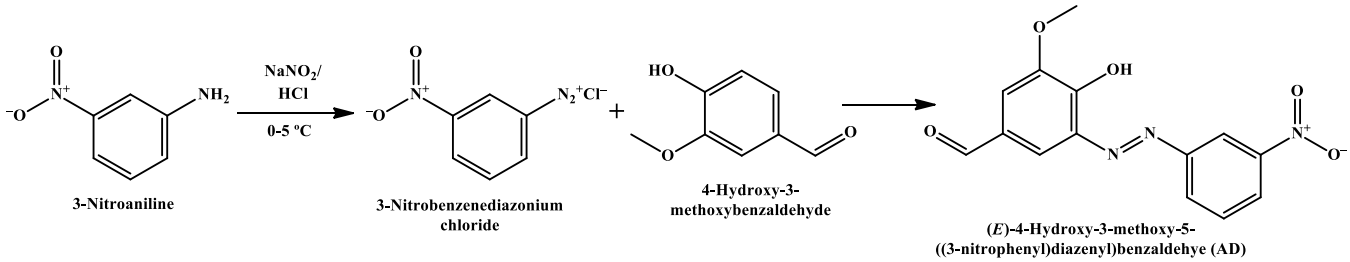

Scheme-I: Schematic representation of the chemical reactions involved in the synthesis of dye AD

environment. B3LYP/6-311++G(d,p) provides a great balance between computational efficiency and accuracy for modelling HOMO-LUMO gaps and charge transfer in azo dyes [43]. Polarizable Continuum Model (PCM), which treats solvents as a continuous polarizable medium, can capture the ethanol-induced shifts in the electronic spectra and also stabilizes charge-separated states in TD-DFT calculations [44].

No imaginary frequencies were found. The electronic spectra of the optimized structures were computed by TD-DFT at the same level of theory in ethanol using the PCM model. The ^{1}H and ^{13}C NMR spectra of the optimized structure in DMSO were calculated using the GIAO method. To understand the origin of the transitions, molecular orbital analysis of the tautomeric and the deprotonated form of the dye was performed. Experimental and theoretical results for NMR, IR and UV-vis were correlated and statistical analysis was performed to predict the suitability of the computational studies. The R^2 (coefficient of determination) and RSDM (root mean squared deviation) values were calculated.

RESULTS AND DISCUSSION

This study explores the structure of the synthesized compound AD and its ability to function as a pH sensor. The dye is synthesized by the conventional diazo coupling reaction. ^{1}H NMR, ^{13}C NMR, CHN analysis, ATR IR and mass spectrometry have been used to characterize the synthesized dye. The *ortho* hydroxyl azo dyes exhibit intramolecular hydrogen bonding and may exist as the azo or hydrazone tautomer or an equilibrium mixture of the two. Since the dye is soluble in ethanol, the computational studies were carried out in the gas phase and in ethanol. The experimental and computed results have been compared.

Structure and conformational analysis: The optimized structure of dye AD (azo tautomer), at the B3LYP/6-311++G (d,p) in ethanol, is shown in Fig. 1. The FTMS + p ESI spectrum is presented in Fig. 2. The $[M+H]^+$ obtained at 302.07 confirms the formation of the dye AD. Table-1 lists the proposed fragments observed in an FTMS + p ESI spectrum of AD.

Azo compounds with a hydroxyl group conjugated with the azo group exhibit tautomerism [45]. This holds true if the OH group is *ortho* or *para* to the azo group [46,47]. The proton of the hydroxyl group is labile and migrates to the nitrogen of the azo group, establishing an equilibrium between the azo and hydrazone form [46]. In dyes where tautomerism exists, one tautomer may be dominant under a set of conditions or both may exist in equilibrium [3,48,49]. However, an electron-donating group favours the enolic form and an electron-withdrawing favours the ketonic form. Hydrogen bonding to the solvent and steric hindrance in a molecule also affect the stab-ility of the tautomers [50]. A relaxed potential energy surface scan at the B3LYP/6-311++G(d,p) level of theory was used to find the most stable conformer of dye AD in the gas phase and ethanol. All geometrical parameters were simultaneously relaxed while the dihedral angle C_5-N_{18}-N_{19}-C_{20} was scanned. The variation in energy (gas phase/ethanol) *vs.* the dihedral angle is shown in Fig. 3. The hydroxyl hydrogen (*ortho* to azo linkage) is within hydrogen bonding distance to the azo nitrogen. As the dihedral angle is scanned, the azo tautomer converts to the hydrazone tautomer. This was true for the gas phase scan and the scan with ethanol as the medium. The lowest energy structure is obtained for the azo tautomer in ethanol. The azo form is slightly more stable than the hydrazone form by 0.1757 kcal/mol in ethanol. The structures (gas phase/ethanol) and energy values for the azo and hydrazone tautomers are depicted in Fig. 3. The small energy difference between the tautomers suggests that the azo and hydrazone forms may exist in equilibrium in solution.

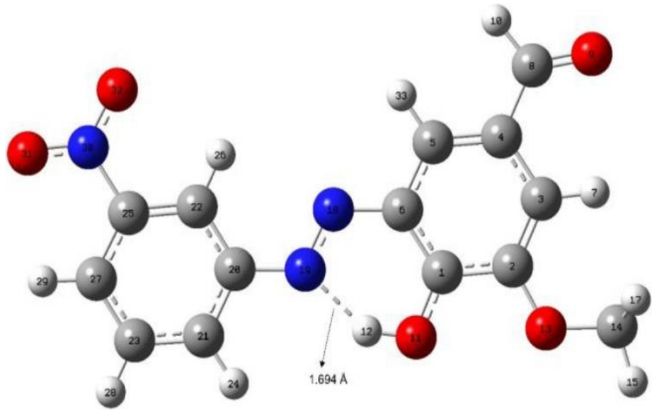

Fig. 1. The optimized structure of AD

TABLE-1
PROPOSED FRAGMENTS OBSERVED IN AN
FTMS + p ESI SPECTRUM OF AD DYE MOLECULE

m/z	Proposed fragment
302.07	$[M+H]^+$
246.86	$C_{14}HO_4N$
205.99	$C_{12}O_3N$
182.98	$C_5HO_5N_3$
155.97	$C_4O_5N_2$
141.96	C_4O_5N
132.96	$C_2HO_5N_2$

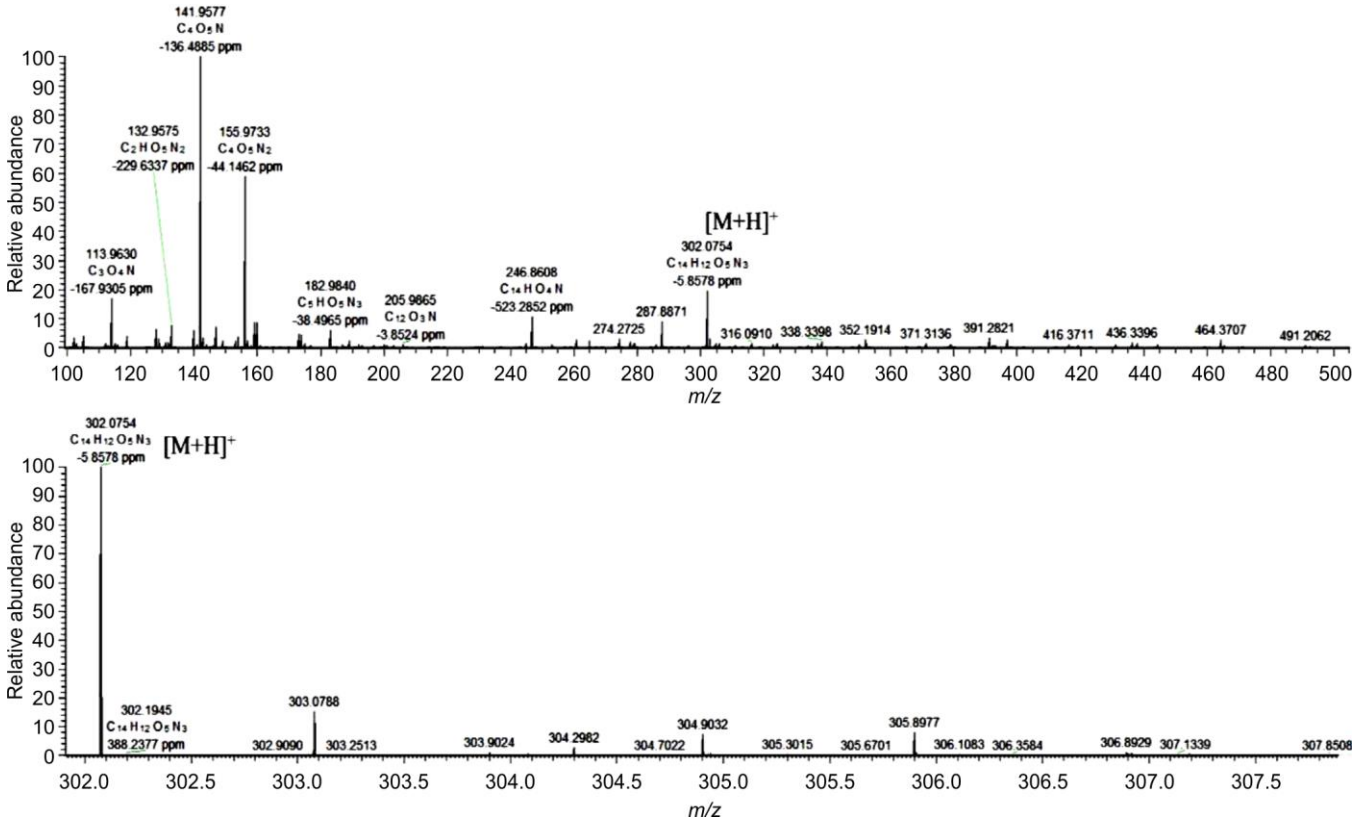

Fig. 2. Mass spectrum (p-ESI) of AD dye molecule

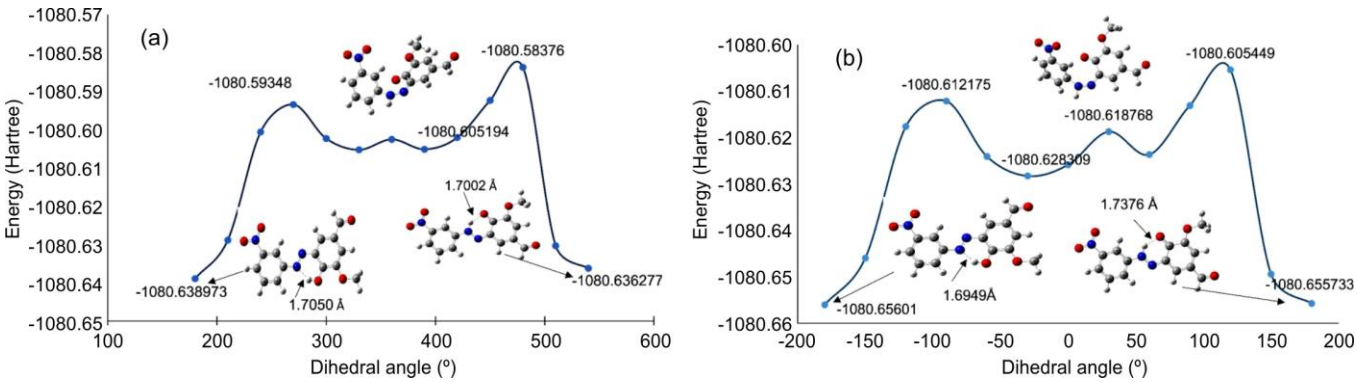

Fig. 3. PES scan for dihedral angle C_5-N_{18}-N_{19}-C_{20} of the dye AD by B3LYP/6-311++g(d,p) method in the (a) gas phase and (b) ethanol

IR spectral analysis: The ATR-IR spectrum of the dye was recorded between 4000-400 cm^{-1}. The major IR bands are displayed in Fig. 4. The absence of a broad strong signal associated with the hydroxyl group in the infrared spectrum suggests that the hydrazone form may dominate in the solid state [43]. The vibrational frequencies obtained at the B3LYP /6-311++g(d,p) level of theory were scaled by 0.967 [47,51]. The R^2 value of 0.9952 indicates an almost linear relationship, suggesting the theoretical model (after scaling) is good at predicting the IR frequencies. The RMSD value of 48.64 cm^{-1} is a reasonable error margin [51,52]. The highest contributor to the error being the C–H (CHO) stretch. The computed and experimental infrared frequencies were compared and the results are summarized in Table-2.

NMR spectral analysis: The structure of AD was further verified by recording the ^1H and ^{13}C NMR spectra in DMSO-d_6 (Fig. 5). The hydroxyl proton appears as a singlet δ 11.6 (s, 1H, OH) and the computed spectra for the optimized structure using the GIAO method predicted a chemical shift value of 14.2.

TABLE-2
EXPERIMENTAL AND COMPUTED IR FREQUENCIES FOR AD DYE MOLECULE

IR stretching frequencies (cm^{-1})	Experimental	Theoretical (scaled) (azo)
NO_2 symmetric stretch	1348	1357
N-N	1525	1524
C=O(CHO)	1673	1716
NO_2 asymmetric stretch	1589	1553
C-H (CHO)	2834	2932
O-H	3097 (weak)	3116
C-H(CH_3)	–	3020

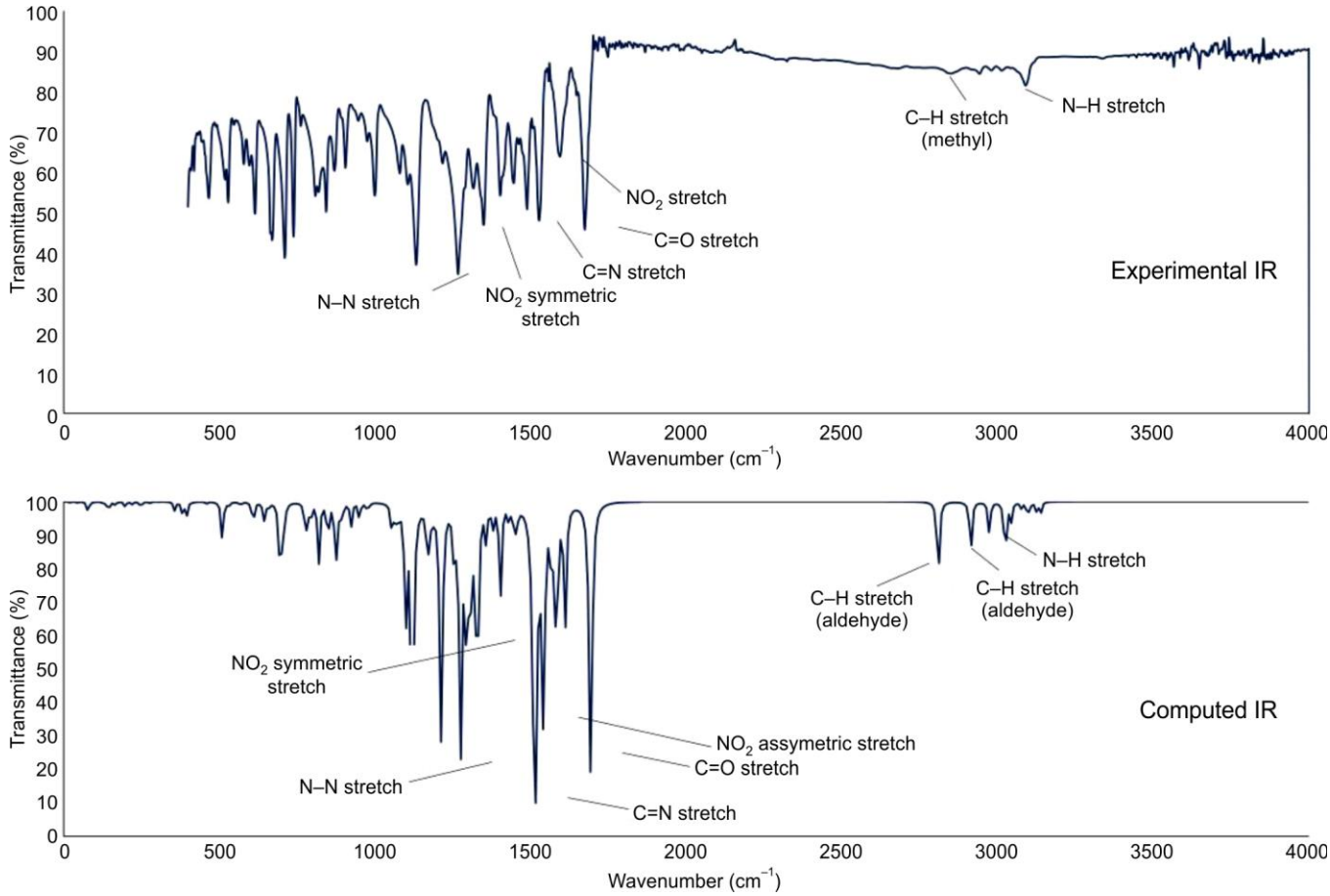

Fig. 4. Experimental and computed IR spectra for AD dye molecule

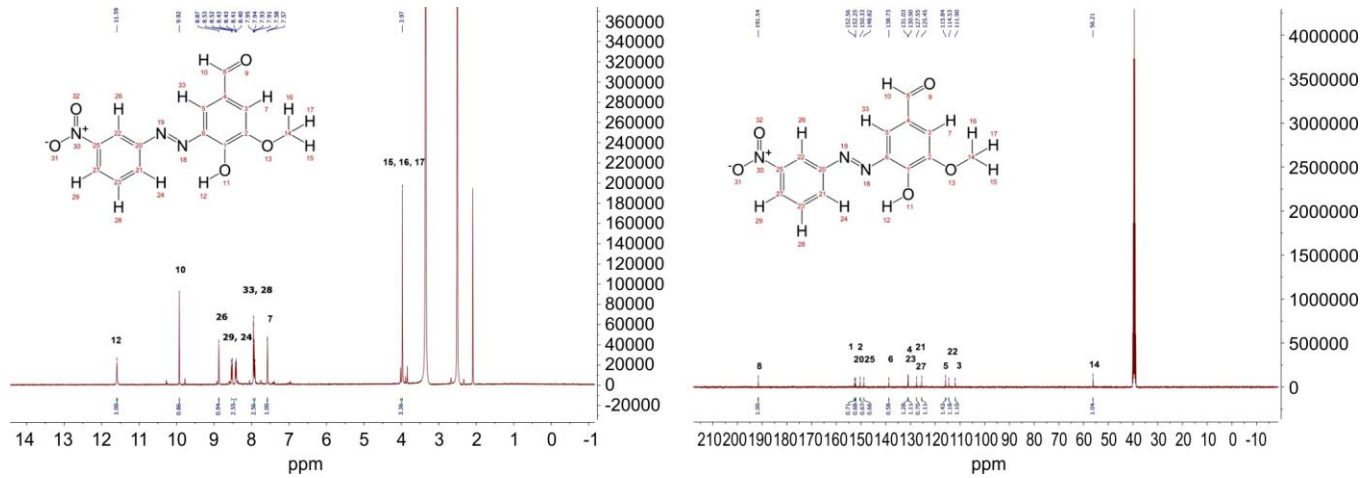

Fig. 5. ^{1}H NMR and ^{13}C NMR spectra of AD dye molecule in DMSO-d_6 solvent

The aldehyde proton appears at δ 9.9 (s, 1H, CHO), close to the computed value of δ 10.1. The methyl protons appear at δ 3.97 (s, 3H, OCH_3). The aromatic protons resonate between δ 7.5-8.5 (m, Ar–H) as multiplets and matched well with the computed values. The ^{13}C NMR spectrum of AD compound shows characteristic peaks for the aldehyde carbon at δ 191.5 (CHO), which is close to the theoretically calculated value of δ 197.8. The methoxy carbon appears at δ 56.2 (OCH_3), close to the computed value of δ 56.2 (OCH_3). The hydroxy substituted aromatic carbon, which is important for the identification of the compound, appears at δ 152.5 (C–OH) [53]. Table-3 compares the computed and experimental ^{1}H NMR and ^{13}C NMR chemical shift values. The R^2 and RMSD for the ^{1}H NMR are 0.981 and 0.834 ppm and ^{13}C NMR are 0.957 and 9.32 ppm, respectively.

pH-dependent spectrophotometric response correlation of experimental and computational studies: The spectrum of the AD dye (3×10^{-4} M) in ethanol is presented in Fig. 6. The computed absorption spectra for the azo and hydrazone forms of AD obtained by TD-DFT at the same level of theory

TABLE-3
EXPERIMENTAL AND COMPUTED (B3LYP/6-311++g(d,p)/GIAO) ^{1}H AND ^{13}C ISOTROPIC CHEMICAL SHIFTS (Δ, ppm) WITH TMS AS REFERENCE

Atoms	Experimental chemical shift value (ppm)	Theoretical chemical shift value (ppm)
H_{12}	11.5905	14.2776
H_{10}	9.9248	10.1032
H_{26}	8.8696	9.2189
H_{29}	8.52385	8.6342
H_{24}	8.4184	8.5906
H_{33}	7.94495	8.1743
H_{28}	7.9158	7.9074
H_{7}	7.57465	7.5855
H_{15}	4.0194	4.459
H_{16}	3.9711	3.9715
H_{17}	3.8891	3.9703
C_{8}	191.5363	197.8689
C_{20}	152.2508	157.3888
C_{1}	152.5594	156.7721
C_{25}	148.8249	156.0341
C_{2}	150.3281	155.7469
C_{21}	127.5514	144.4335
C_{6}	138.7315	142.3708
C_{5}	115.8379	141.6071
C_{23}	130.9029	135.9167
C_{4}	131.0269	134.2025
C_{27}	125.4513	131.4807
C_{22}	114.5325	114.2556
C_{3}	111.9039	113.9151
C_{14}	56.2081	57.925

in ethanol are compared with the experimentally obtained spectrum of dye in ethanol (Fig. 6). The computational study on the azo AD dye and hydrazone tautomers in ethanol reveals that both the azo and enol forms can exist in equilibrium in the solution. The solution of the dye in ethanol is yellow-orange in colour. The experimentally obtained spectra in ethanol show a broad absorption spectrum encompassing the absorption regions of both azo and hydrazone forms. Hydrogen bonding, pH, dilution effects, substituent effects, solvents, crystallization and nanocage effects influence the tautomerism in azo dyes [47]. The geometry-optimized structure reveals that the hydroxyl hydrogen is in hydrogen bonding distance to the azo nitrogen (1.6952 Å) and locks the molecule in the trans- conformation in the azo form. The dipole moment of the push-pull type molecule is fairly large, 6.68148 D. In the hydrazone form, the NH group is also within hydrogen bonding distance to the oxygen (1.7376 Å). The dipole moment is computed to be 6.3523 D. Hydrogen bonding diminishes the electron density on the azo nitrogen, making the molecule stable towards photochemical oxidation.

A simple experiment was designed to examine the colour of compound AD under different pH conditions. The hydroxyl substituent in AD is expected to make the dye pH-responsive. Under basic conditions *i.e.*, high pH values, the hydrogen ions participating in hydrogen bonding are lost, forming the enolate ion [47,54]. A simple visual comparison of the dye colour in the buffer solutions spanning a range of pH values from 1-13 revealed two distinct colours, yellow and orange (Fig. 7a). The change in colour from yellow to orange corresponds to a transition from an acidic to a basic solution, the colour orange, first appearing at pH 7. The proposed structures under acidic and alkaline conditions are depicted in Fig. 7b. The colour change is attributed to the deprotonation of the hydroxyl group in the basic medium. The UV/visible spectra of AD in a series of buffer solutions are presented in Fig. 7c. New absorbance peaks develop in the basic region.

The predicted absorption spectra of the protonated (azo) and the deprotonated form of AD (enolate ion) to simulate the effect of low and high pH values are presented in Fig. 6a. The experimental UV/vis spectrum of AD under acidic conditions mirrors the theoretically predicted spectrum of the azo form in ethanol, the spectrum in the basic medium resemble the spectrum of the deprotonated form (high pH). The structure of the deprotonated form at RB3LYP functional using 6-311++G (d,p) basis sets in ethanol applying the polarizable continuum model (PCM) is presented in Fig. 7d. Table-4 compares the computed and experimental UV-vis spectra of the azo, hydrazone and enolate ion forms of the dye. The R^2 and RMSD values were calculated for the enolate ion form (R^2 = 0.996; RMSD = 3.995 nm). These values indicate a good correlation and only a slight deviation between the theoretical and experimental spectra. In contrast, the azo form observed under low

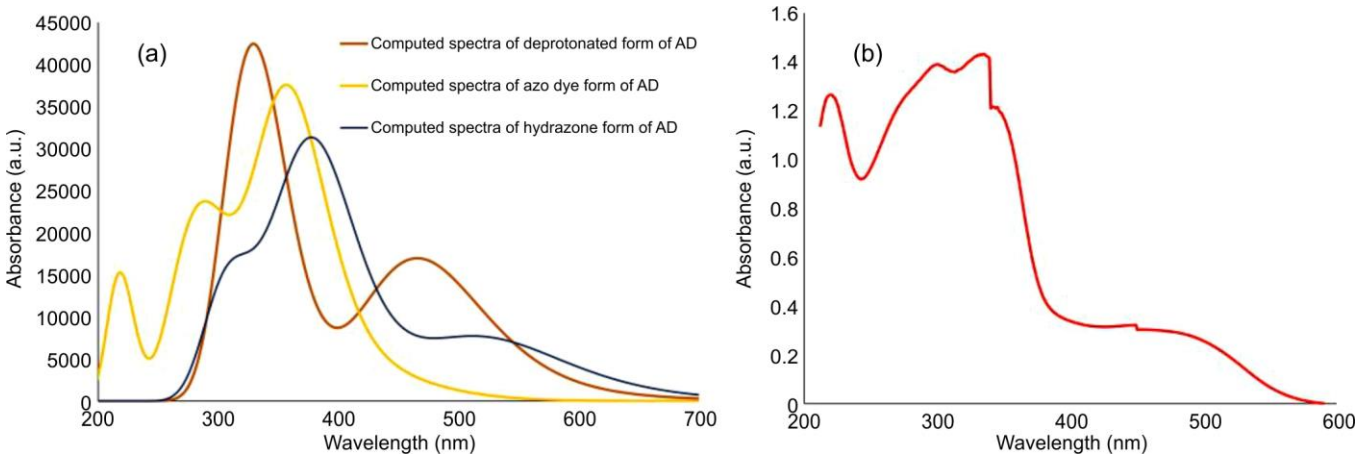

Fig. 6. (a) Computed electronic absorption spectra (TD-DFT) of the azo (enolic) and hydrazone (ketonic) tautomers and enolate forms of AD using DFT, (b) the electronic absorption spectrum of AD (3×10^{-3} M) in ethanol

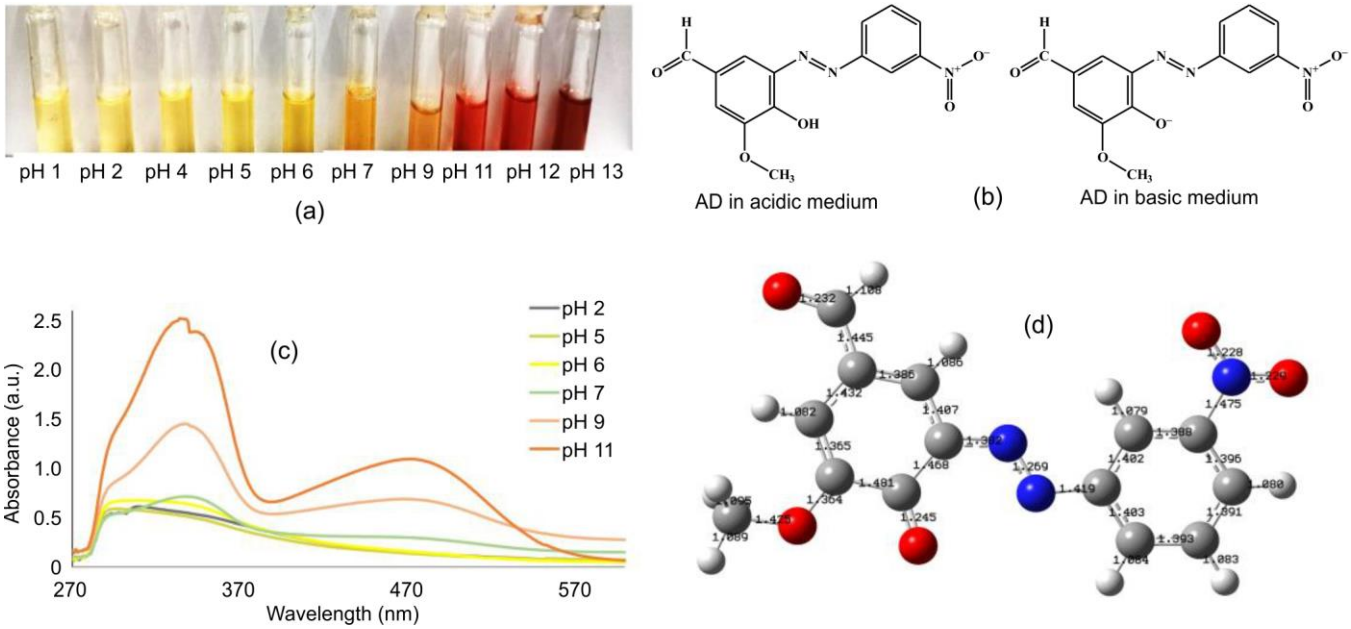

Fig. 7. (a) Colour of AD dye in buffer solutions (pH:1-13), (b) proposed structures of AD molecule in the acidic and basic media, (c) electronic absorption spectra of AD molecule at different pHs, and (d) geometry optimized structure of the enolic form of AD dye molecule

TABLE-4
COMPUTED AND EXPERIMENTALLY OBSERVED ABSORPTION PEAK VALUES OF THE AD DYE MOLECULE

λ-Ethanol (experimental)	λ (computed)			λ (experimental)	
	Azo	Hydrazone	Enolate ion	Acidic medium	Basic medium
Broad absorption from 300-560 nm with peaks at 225 nm, 303 nm, 350 nm, broad band centered around 456 nm	216.98 nm, 304.35 nm, 357.37 nm	217.6 nm, 312.57 nm, 380.99 nm, 522.11 nm	339.16 nm, 466.41 nm	Broad absorption peak 300-360 nm	340 nm, 472 nm

pH conditions exhibited a broad absorption peak, making quantitative spectral fitting impractical. It can, however, be concluded that good accuracy and reliability are obtained at this level of theory.

To understand the electronic properties of the molecule in the acidic and basic medium, the molecular orbitals and their energy values are presented in Fig. 8. The π-π* transitions for the azo, hydrazone and enolate ion forms are observed in the 300-360 nm range. The band at 522 nm for the hydrazone form has a major contribution from the HOMO-LUMO transition which is a π-π* transition. The enolate ion form, with a peak at 466 nm, is a mix of transitions from HOMO-LUMO+1 and HOMO-1 – LUMO+1. In the enolate ion form, the HOMO is centered on the vanillin moiety and the LUMO on the nitrobenzene ring. The energy gap between the HOMO and LUMO is 3.37 eV for the azo tautomer, 2.82 eV for the hydrazone tautomer and 2.33 eV for the enolate ion. The molecular orbitals contributing to the observed transitions, the excitation energies, coefficients, wavelength and oscillator strength for the major transitions are presented in Table-5. The computed and experimental spectra correlate well.

Acid-base titrations were performed to assess the suitability of the indicator for a strong acid *vs*. a strong base titration. Titrations of various concentrations of HCl and oxalic acid against NaOH, as listed in Table-6, were performed to ascertain the suitability of the AD molecule indicator in dilute and concentrated solutions and at various acid-to-base ratios. A comparison was made with phenolphthalein as an indicator. A strong acid *vs*. strong base titration has a sharp end equivalence point near pH 7. The most suitable indicator for this titration should have a pK_a value close to the equivalence point. The pK_a value of AD in 10% ethanol is found to be 6.72 ± 0.02 by the method proposed by Fan *et al.* [55]. The colour stability of the indicator was also determined. Consistent results were obtained using AD compound as an indicator. On applying the t-test, no statistically significant variation was found between AD and phenolphthalein indicators in the volume required for neutralization, suggesting that both are reliable.

Conclusion

In this study, a new compound, (*E*)-4-hydroxy-3-methoxy-5-((3-nitrophenyl)diazenyl)benzaldehyde (AD) and characterized with CHN analysis, NMR, FT-IR, HR-MS and DFT calculations. The dye exhibits a distinct, reversible colour change in response to pH, which is driven by the processes of protonation and deprotonation at the phenolic group. This alteration in electronic structure, validated by both experimental findings and theoretical models, provides the dye with a consistent and predictable response suitable for acid–base titrations. Azo dyes are widely used as indicators for weak acid–strong base titrations, offering sharp and distinct end points. Compared to phenolphthalein, which is colourless in acidic and near-neutral solutions and only develops a pink colour above pH 8.3, the synthesized dye provides a distinct yellow-to-orange transition

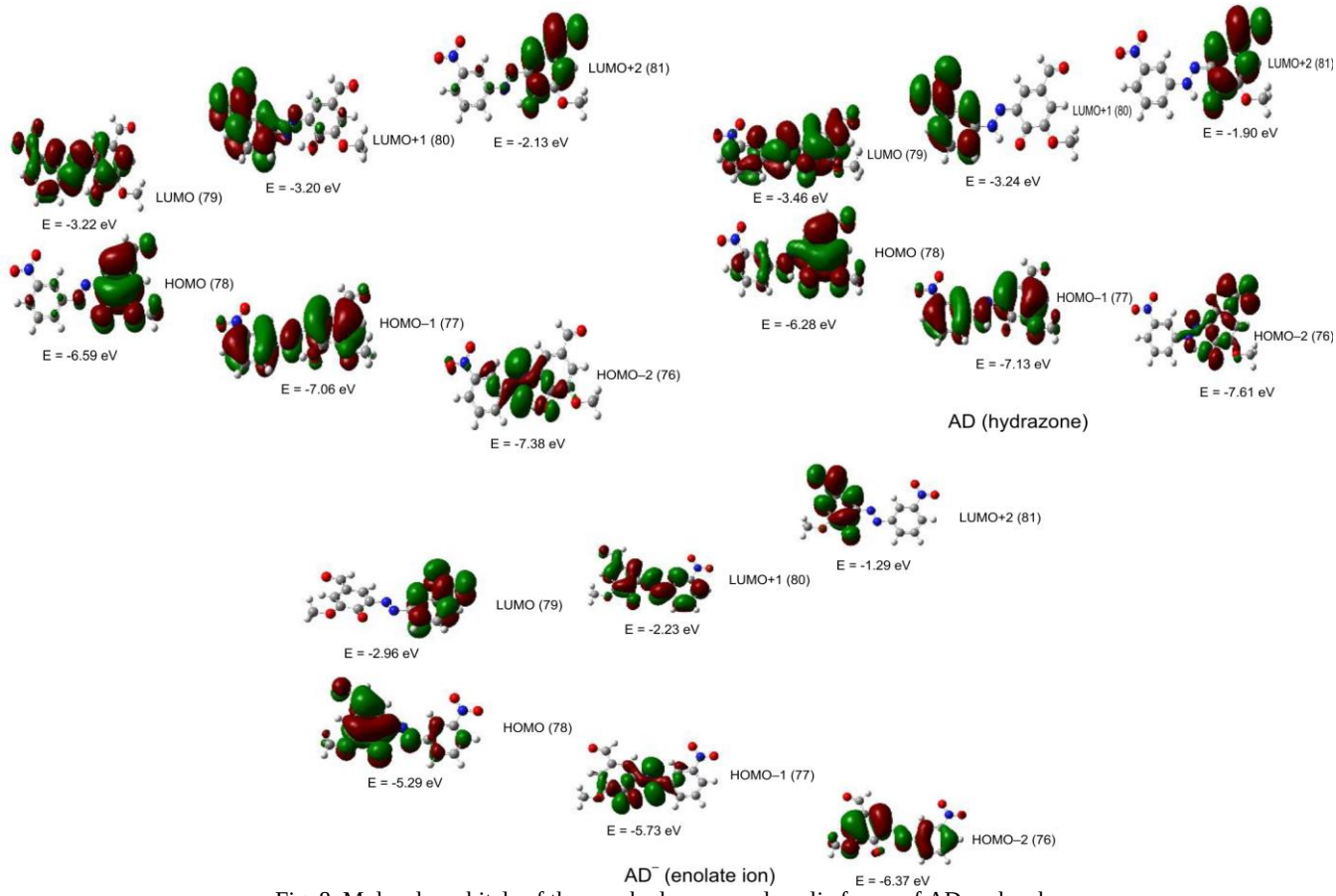

Fig. 8. Molecular orbitals of the azo, hydrazone and enolic forms of AD molecule

TABLE-5
EXCITATION ENERGIES AND OSCILLATOR STRENGTHS OF MAJOR TRANSITIONS OF AZO, HYDRAZONE AND ENOLIC FORMS OF THE DYE AD MOLECULE

Molecular orbitals involved in transitions	Excitation energy (eV)	Wavelength (nm)	Coefficients	Oscillator strength
AD (Azo tautomer)				
Excited state 2: Singlet-A	2.8068	441.72		0.0572
78 → 79			0.68381	
78 → 80			0.14542	
Excited state 5: Singlet-A	3.4693	357.37		0.7977
77 → 79			0.55503	
77 → 80			0.42662	
Excited state 11: Singlet-A	4.0738	304.35		0.2537
77 → 81			-0.24075	
78 → 81			0.64182	
Excited state 14: Singlet-A				
77 → 81			0.63203	
78 → 81			0.2538	
Excited state 17: Singlet-A	4.6091	269		0.1353
73 → 79			0.48743	
73 → 80			-0.42535	
74 → 79			-0.13811	
74 → 80			-0.16432	
Excited state 26: Singlet-A	5.6524	219.35		0.152
73 → 81			0.1496	
74 → 81			-0.18952	
77 → 82			-0.16801	
78 → 83			0.60758	
Excited state 28: Singlet-A	5.7142	216.98		0.1526
69 → 79			0.11777	
73 → 81			0.45933	
77 → 82			-0.38281	
77 → 83			0.1689	
78 → 83			-0.22962	

AD (Hydrazone)				
Excited state 1: Singlet-A	2.3747	522.11		0.1811
77 → 79			-0.12539	
78 → 79			0.69564	
Excited state 4: Singlet-A	3.2543	380.99		0.689
77 → 79			0.6774	
77 → 80			-0.13858	
78 → 79			0.12479	
Excited state 9: Singlet-A	3.9667	312.57		0.3178
73 → 79			-0.14864	
74 → 79			0.11292	
77 → 81			-0.10496	
78 → 81			0.66055	
Excited state 13: Singlet-A	4.3321	286.2		0.1263
73 → 79			0.12621	
74 → 80			0.67717	
Excited state 29: Singlet-A	5.6976	217.61		0.1619
66 → 79			0.22479	
69 → 79			0.23068	
74 → 83			0.13503	
77→ 82			0.40603	
77 → 83			0.21505	
78 → 83			-0.1032	
78 → 85			-0.35198	
Enolate ion (AD)				
Excited state 4: Singlet-A	2.6583	466.41		0.4093
77 → 80			-0.12898	
78 → 80			0.69036	
Excited state 8: Singlet-A	3.6557	339.16		0.4193
76 → 80			0.6635	
78 → 81			0.20766	
Excited state 10: Singlet-A	3.8299	323.72		0.6177
71 → 79			0.15871	
74 → 80			0.14521	
76 → 80			-0.19914	
78 → 81			0.62131	

TABLE-6
TITRATION DATA FOR HCl AND $C_2O_4H_2$ *vs*. NaOH (STRONG ACID *vs*. STRONG BASE TITRATIONS) USING PHENOLPHTHALEIN AND DYE AD AS AN INDICATOR

Average volume of the NaOH solution(mL) ± SD	Indicator	95% Confidence interval for mean difference	Colour before the endpoint	Colour at the endpoint	Colour stability
0.01 N HCl against 0.01 N NaOH (calculated)					
9.0 ± 0.0	AD	± 0.00	Yellow	Orange	Permanent
9.0 ± 0.0	Phenolphthalein		Colourless	Pink	Permanent
0.1 N HCl against 0.1 N NaOH (calculated)					
8.87 ± 0.05	AD	± 0.08	Yellow	Orange	Permanent
8.9 ± 0.0	Phenolphthalein		Colourless	Pink	Permanent
0.5 N HCl against 0.5 N NaOH (calculated)					
8.26 ± 0.057	AD	± 0.09	Yellow	Orange	Permanent
8.23 ± 0.057	Phenolphthalein		Colourless	Pink	Permanent
1 N HCl against 1N NaOH (calculated)					
9.2 ± 0.0	AD	± 0.08	Yellow	Orange	Permanent
9.17± 0.05	Phenolphthalein		Colourless	Pink	Permanent
0.1N HCl against 0.2 N NaOH (calculated)					
4.6 ± 0.0	AD	± 0.04	Yellow	Orange	Permanent
4.58 ± 0.02	Phenolphthalein		Colourless	Pink	Permanent
0.1N HCl against 0.5 N NaOH (calculated)					
1.8 ± 0.05	AD	± 0.06	Yellow	Orange	Permanent
1.8 ± 0.0	Phenolphthalein		Colourless	Pink	Permanent

0.01 N $H_2C_2O_4$ against 0.01 N NaOH (calculated)					
8.17 ± 0.05	AD	± 0.08	Yellow	Orange	Permanent
8.16 ± 0.05	Phenolphthalein		Colourless	Pink	Permanent
0.1 N $H_2C_2O_4$ against 0.1 N NaOH (calculated)					
8.8 ± 0.0	AD	± 0.00	Yellow	Orange	Permanent
8.8 ± 0.00	Phenolphthalein		Colourless	Pink	Permanent
0.5 N $H_2C_2O_4$ against 0.5 N NaOH (calculated)					
10.33 ± 0.057	AD	± 0.09	Yellow	Orange	Permanent
10.37 ± 0.05	Phenolphthalein		Colourless	Pink	Permanent
0.1N $H_2C_2O_4$ against 0.2 N NaOH (calculated)					
5.05 ± 0.057	AD	± 0.09	Yellow	Orange	Permanent
5.075 ± 0.05	Phenolphthalein		Colourless	Pink	Permanent
0.1N a $H_2C_2O_4$ against 0.5 N NaOH (calculated)					
1.95 ± 0.057	AD	± 0.06	Yellow	Orange	Permanent
1.9 ± 0.0	Phenolphthalein		Colourless	Pink	Permanent

beginning near neutral pH and maintains consistent endpoint visibility across a range of acid–base titrations, making it a promising and potentially more versatile alternative for certain analytical applications. This study demonstrates that the minor structural changes such as nitro substitution and the addition of an aldehyde group, can finely tune the colour response and solvent interactions of azo dyes. While the findings highlight the AD dye's potential, the study was limited to the controlled laboratory conditions without evaluating long-term stability or interference from other substances. Future work will focus on enhancing pH sensitivity, improving stability under light and heat, and integrating the dye into practical formats like films, test strips or sensors for real-world applications.

ACKNOWLEDGEMENTS

The authors are sincerely grateful to the Principal, St. Stephen's College, Delhi, India, for his support. The authors are grateful to the University Science Instrumentation Centre, Delhi University for providing necessary instrumentation facilities to facilitate the work. Sincere gratitude to Dr. Yashwant Kumar (Senior Research Scientist) and Sonu Kumar Gupta (Ph.D. Scholar), from Translational Health Science and Technology Institute, DBT-GOI for carrying out the mass spectral analysis.

CONFLICT OF INTEREST

The authors declare that there is no conflict of interests regarding the publication of this article.

REFERENCES

1. S. Benkhaya, S. M'rabet and A. El Harfi, *Heliyon*, **6**, e03271 (2020); https://doi.org/10.1016/j.heliyon.2020.e03271
2. R.I. Alsantali, Q.A. Raja, A.Y.A. Alzahrani, A. Sadiq, N. Naeem, E.U. Mughal, M.M. Al-Rooqi, N. El Guesmi, Z. Moussa and S.A. Ahmed, *Dyes Pigments*, **199**, 110050 (2022); https://doi.org/10.1016/j.dyepig.2021.110050
3. A.Z. Omar, A.M. Khamis, E.A. Hamed, S.K. El-Sadany, E.M. Abdel Rehim, M.E. Elba, M.G. Mohamed and M.A. El-Atawy, *Sci. Rep.*, **13**, 21554 (2023); https://doi.org/10.1038/s41598-023-48368-y
4. J. Garcia-Amorós, M.C.R. Castro, S. Nonell, S. Vílchez, J. Esquena, M.M.M. Raposo and D. Velasco, *J. Phys. Chem. C*, **123**, 23140 (2019); https://doi.org/10.1021/acs.jpcc.9b07527
5. S.W. Oh, J.M. Baek, S.H. Kim and T.H. Yoon, *RSC Adv.*, **7**, 19497 (2017); https://doi.org/10.1039/C7RA01507K
6. S. Atkins, A. Chueh, T. Barwell, J.M. Nunzi and L. Seroude, *Sci. Rep.*, **10**, 3267 (2020); https://doi.org/10.1038/s41598-020-60245-6
7. M. Di Martino, L. Sessa, R. Diana, S. Piotto and S. Concilio, *Molecules*, **27**, 3712 (2023); https://doi.org/10.3390/molecules28093712
8. P.J. Coelho, L.M. Carvalho, J.C.V.P. Moura and M.M.M. Raposo, *Dyes Pigments*, **82**, 130 (2009); https://doi.org/10.1016/j.dyepig.2008.12.005
9. Y. Liu, C. Xiong, L. Dong, Y. Niu, L. Liu and Q. Zhu, *J. Wuhan Univ. Technol. Mater. Sci. Ed.*, **25**, 979 (2010); https://doi.org/10.1007/s11595-010-0133-9
10. R. Gester, A. Torres, C. Bistafa, R.S. Araújo, T.A. da Silva and V. Manzoni, *Mater. Lett.*, **280**, 128535 (2020); https://doi.org/10.1016/j.matlet.2020.128535
11. D.Z. Mutlaq, Q.M.A. Hassan, H.A. Sultan and C.A. Emshary, *Opt. Mater.*, **113**, 110815 (2021); https://doi.org/10.1016/j.optmat.2021.110815
12. D.S. Patil, K.C. Avhad, M.M. Kadam and N. Sekar, *SN Appl. Sci.*, **1**, 259 (2019); https://doi.org/10.1007/s42452-019-0268-z
13. P.M.R. Batista, C.D.F. Martins, M.M.M. Raposo and S.P.G. Costa, *Molecules*, **26**, 3326 (2023); https://doi.org/10.3390/molecules28083326
14. M. Patel, A.R. Likhar, A.K. Bhojani, A. Vaishnani, H. Patel, D.K. Singh, D. Asthana and N. Gour, *Microchem. J.*, **200**, 110351 (2024); https://doi.org/10.1016/j.microc.2024.110351
15. S. Kamali, R. Arabahmadi, M. Orojloo and S. Amani, *Microchem. J.*, **184**, 108204 (2023); https://doi.org/10.1016/j.microc.2022.108204
16. A. Sayqal, M.M. Alotaibi, M.A. Kassem and S.A. Ahmed, *Arab. J. Chem.*, **17**, 105686 (2024); https://doi.org/10.1016/j.arabjc.2024.105686
17. K. Mezgebe and E. Mulugeta, *RSC Adv.*, **12**, 25932 (2022); https://doi.org/10.1039/D2RA04934A
18. Y. Ali, S.A. Hamid and U. Rashid, *Mini Rev. Med. Chem.*, **18**, 1548 (2018); https://doi.org/10.2174/1389557518666180524113111
19. M.A. Hissam, Z. Ngaini, N.H. Zamakshshari, F.N.A.M. Hejemi, F.S. Arni and A.N.A. Halim, *Discover Appl. Sci.*, **6**, 325 (2024); https://doi.org/10.1007/s42452-024-05830-4
20. Z. Ngaini, M.A. Hissam, N.A. Mortadza, A.N. Abd Halim and A.I. Daud, *Nat. Prod. Res.*, **38**, 3672 (2023); https://doi.org/10.1080/14786419.2023.2262713
21. K.J. Al-Adilee, S.H. Jawad, H.A.K. Kyhoiesh and H.M. Hassan, *J. Mol. Struct.*, **1295**, 136695 (2024); https://doi.org/10.1016/j.molstruc.2023.136695
22. R.M. Christie, Colour Chemistry, The Royal Society of Chemistry, Cambridge CB4 0WF, UK (2015).

23. M.A. Davasaz Rabbani, B. Khalili and H. Saeidian, *RSC Adv.*, **10**, 35729 (2020); https://doi.org/10.1039/D0RA06934E
24. A. Singh, R. Choi, B. Choi and J. Koh, *Dyes Pigments*, **95**, 580 (2012); https://doi.org/10.1016/j.dyepig.2012.06.009.
25. L.S. Athira, S. Balachandran, J. Annaraj and E.A. Noelson, *J. Mol. Struct.*, **1195**, 556 (2019); https://doi.org/10.1016/j.molstruc.2019.06.007
26. A. Ghanadzadeh Gilani, V. Taghvaei, E. Moradi Rufchahi and M. Mirzaei, *J. Mol. Liq.*, **273**, 392 (2019); https://doi.org/10.1016/j.molliq.2018.10.054
27. H. Zhang, A. Hou, K. Xie and A. Gao, *Sens. Actuators B Chem.*, **286**, 362 (2019); https://doi.org/10.1016/j.snb.2019.01.165
28. S.U. Mestry, V.B. Satalkar and S.T. Mhaske, *Pigm. Resin Technol.*, **53**, 1119 (2023); https://doi.org/10.1108/PRT-05-2023-0039
29. A.A. Noser, S.A. Ibrahim, H.A. Abd El Salam, N.M.A. El-Ebiary and H.S.A. Mandour, *J. Iran. Chem. Soc.*, **20**, 2963 (2023); https://doi.org/10.1007/s13738-023-02891-x
30. Y. Folwill, Z. Zeitouny, J. Lall and H. Zappe, *Liq. Cryst.*, **48**, 862 (2021); https://doi.org/10.1080/02678292.2020.1825842
31. R. Diana, L. Sessa, S. Concilio, S. Piotto, L. Di Costanzo, A. Carella and B. Panunzi, *Crystals*, **14**, 31 (2024); https://doi.org/10.3390/cryst14010031
32. J. Naime, M.S.A. Mamun, M.A.S. Aly, M. Maniruzzaman, M.M.R. Badal and K.M.R. Karim, *RSC Adv.*, **12**, 28034 (2022); https://doi.org/10.1039/D2RA04930A
33. F.L. Coelho, C.Á. Braga, G.M. Zanotto, E.S. Gil, L.F. Campo, P.F.B. Gonçalves, F.S. Rodembusch and F.S. Santos, *Sens. Actuators B Chem.*, **259**, 514 (2018); https://doi.org/10.1016/j.snb.2017.12.097
34. G. Bartwal, K. Aggarwal and J.M. Khurana, *New J. Chem.*, **42**, 2224 (2018); https://doi.org/10.1039/C7NJ04194B
35. B. Purwono, C. Anwar, and A. Hanapi, *Indones. J. Chem.*, **13**, 1 (2013); https://doi.org/10.22146/ijc.21318
36. H. Kahlert, G. Meyer and A. Albrecht, *ChemTexts*, **2**, 7 (2016); https://doi.org/10.1007/s40828-016-0026-4
37. G.H. Jeffery, Vogel's Textbook of Quantitative Chemical Analysis, A John Wiley & Sons, Inc., edn 5 (2022).
38. J. Barbosa, eds.: P. Worsfold, A. Townshend and C.F. Poole, Encyclopedia of Analytical Science, Elsevier, Oxford, edn. 2, pp. 360-371 (2005).
39. F. Melfi, M. Fantacuzzi, S. Carradori, I. D'Agostino, N. Mencarelli, A. Ammazzalorso, M. Gallorini, M. Spano, P. Guglielmi, M. Agamennone, S.H. Ali, A. Al-Samydai and F. Sisto, *RSC Med. Chem.*, **16**, 346 (2025); https://doi.org/10.1039/D4MD00511B
40. P.S.V. Kumar, L. Suresh, T. Vinodkumar, B.M. Reddy and G.V.P. Chandramouli, *ACS Sustain. Chem. Eng.*, **4**, 2376 (2016); https://doi.org/10.1021/acssuschemeng.6b00056
41. M.J. Frisch, G.W. Trucks, H.B. Schlegel, G.E. Scuseria, M.A. Robb, J.R. Cheeseman, G. Scalmani, V. Barone, G.A. Petersson, X. Li, H. Nakatsuji, M. Caricato, V. Marenich, J. Bloino, B.G. Janesko, R. Gomperts, B. Mennucci, H.P. Hratchian, J. V. Ortiz, a. F. Izmaylov, J.L. Sonnenberg, Williams, F. Ding, F. Lipparini, F. Egidi, J. Goings, B. Peng, A. Petrone, T. Henderson, D. Ranasinghe, V.G. Zakrzewski, J. Gao, N. Rega, G. Zheng, W. Liang, M. Ehara, K. Toyota, R. Fukuda, J. Hasegawa, M. Hada, M. Ishida, T. Nakajima, Y. Honda, O. Kitao, H. Nakai, K. Throssell, T. Vreven, J.A. Montgomery Jr., J.E. Peralta, F. Ogliaro, M.J. Bearpark, J.J. Heyd, E.N. Brothers, K.N. Kudin, V.N. Staroverov, T.A. Keith, R. Kobayashi, J. Normand, K. Raghavachari, A.P. Rendell, J.C. Burant, S.S. Iyengar, J. Tomasi, M. Cossi, J.M. Millam, M. Klene, C. Adamo, R. Cammi, J.W. Ochterski, R.L. Martin, K. Morokuma, O. Farkas, J.B. Foresman and D.J. Fox, Gaussian 16 (2016).
42. R. Dennington, T.A. Keith, and J.M. Millam, Semichem Inc.: Shawnee Mission, KS, USA, p. 143 (2016).
43. M. Rizvi, N. Tiwari, A. Mishra and R. Gupta, *ACS Omega*, **7**, 31667 (2022).
44. O.I. Osman, *Int. J. Mol. Sci*., **18**, 239 (2017); https://doi.org/10.3390/ijms18020239
45. Y.H. Ebead, *Dyes Pigments*, **92**, 705 (2012); https://doi.org/10.1016/j.dyepig.2011.06.005
46. B.R. Hsieh, D. Désilets and P.M. Kazmaier, *Dyes Pigments*, **14**, 165 (1990); https://doi.org/10.1016/0143-7208(90)87015-U.
47. M.A. Rauf, S. Hisaindee and N. Saleh, *RSC Adv.*, **5**, 18097 (2015); https://doi.org/10.1039/C4RA16184J
48. J.M.V. Ngororabanga, T.O. Dembaremba, N. Mama and Z.R. Tshentu, *Spectrochim. Acta A Mol. Biomol. Spectrosc.*, **289**, 122202 (2023); https://doi.org/10.1016/j.saa.2022.122202
49. T. Aksungur, Ö. Arslan, N. Seferoğlu and Z. Seferoğlu, *J. Mol. Struct.*, **1099**, 543 (2015); https://doi.org/10.1016/j.molstruc.2015.07.010
50. P. Ball and C.H. Nicholls, *Dyes Pigments*, **3**, 5 (1982); https://doi.org/10.1016/0143-7208(82)80010-7
51. J.P. Merrick, D. Moran and L. Radom, *J. Phys. Chem. A*, **111**, 11683 (2007); https://doi.org/10.1021/jp073974n
52. C. Parlak and P. Ramasami, *SN Appl. Sci.*, **2**, 1148 (2020); https://doi.org/10.1007/s42452-020-2935-5
53. L.A. Fedorov, *Russ. Chem. Rev.*, **57**, 941 (1988); https://doi.org/10.1070/RC1988v057n10ABEH003403
54. L. Van der Schueren, K. Hemelsoet, V. Van Speybroeck and K. De Clerck, *Dyes Pigments*, **94**, 443 (2012); https://doi.org/10.1016/j.dyepig.2012.02.013
55. J. Fan, X. Shen, and J. Wang, *Anal. Chim. Acta*, **364**, 275 (1998) https://doi.org/10.1016/S0003-2670(98)00039-7